Environmental Science Nano

Modeling Reactive Transport of Polydisperse Nanoparticles: Assessment of the Representative Particle Approach

Journal:	*Environmental Science: Nano*
Manuscript ID	EN-ART-06-2018-000666.R1
Article Type:	Paper
Date Submitted by the Author:	28-Aug-2018
Complete List of Authors:	Taghavy, Amir; University of Massachusetts Dartmouth College of Engineering, Civil and Environmental Engineering Abriola, Linda; Tufts University, Department of Civil and Environmental Engineering

SCHOLARONE™
Manuscripts

Environmental Significance Statement

Title: Modeling Reactive Transport of Polydisperse Nanoparticles: Assessment of the Representative Particle Approach

Authors: Amir Taghavy [1], and Linda M. Abriola[2,*]

[1] Department of Civil and Environmental Engineering, University of Massachusetts Dartmouth, MA, 02747

[2] Department of Civil and Environmental Engineering, Tufts University, Medford, MA 02155

Many nanoparticle suspensions that enter the subsurface environment are polydisperse mixtures, and for other (monodisperse) suspensions, polydispersity often evolves through *in situ* processes, including agglomeration and dissolution. Despite this inherent variation of particle sizes, however, conventional approaches to modeling the fate and transport of nanoparticles in porous media typically employ a population mean size (representative diameter) to predict nanoparticle mobility and reactivity. In this work, we explore the nature and extent of potential errors introduced by the use of a 'representative particle approach' (RPA) in the prediction of reactive nanoparticle transport. Here comprehensive analyses are conducted to quantify the uncertainty associated with RPA predictions of silver nanoparticle filtration, oxidative dissolution, and silver ion elution under representative environmental conditions. Results of this investigation suggest that use of the RPA for environmental risk assessment or the design/assessment of subsurface remedial strategies that involve nanoparticles can lead to signification of errors in transport predictions, contributing to uncertainty in estimated risk or the efficacy of a design.

Title: Modeling Reactive Transport of Polydisperse Nanoparticles: Assessment of the Representative Particle Approach

Authors: Amir Taghavy [1], Linda M. Abriola[2,*]

[1] Department of Civil and Environmental Engineering, University of Massachusetts Dartmouth, MA, 02747

[2] Department of Civil and Environmental Engineering, Tufts University, Medford, MA 02155

Abstract:

Objective: Our goal was to characterize the uncertainty in the estimates of the mobility and reactivity of polydisperse nanocolloids introduced into computations when a distribution of particle sizes is replaced with a representative particle diameter through ensemble averaging.

Methods: An existing colloid and solute transport simulator was modified to account for size distribution of injected particles and was used to model the elution of dissolving silver nanoparticles in 1D porous media in both simplified (ensemble averaging) and more realistic (polydisperse) simulations. Laboratory data on nano-silver dissolution, transport, and size distribution were incorporated from the existing literature.

Results: The representative particle approach (RPA) systematically underestimated silver ion speciation and elution (~10-15% error in all RPA simulations that incorporated experimental size distribution data). RPA resulted in an underestimation of particulate silver elution in some simulated case scenarios but yielded overestimates in other cases. At a reduced interstitial velocity of 0.7 m/d, RPA underestimated silver elution in both particulate and ionic forms (an overall -6% error in total silver elution estimate). The magnitude of RPA errors was found to correlate positively with the skewness of size distribution, but exhibited a non-monotonic and less sensitive functional dependence on distribution mean.

Conclusions: Our analysis suggests the absolute RPA error in the particulate and total silver mobility estimates to be less than 5% under the conditions of laboratory column experiments and limited to 10% under the flow conditions of shallow sandy aquifers. For generic highly skewed and bimodal size distributions, RPA estimates fell outside a 10% error margin, demonstrating the importance of incorporating size distribution data in simulations of polydisperse nanoparticles exhibiting highly skewed and/or multi-modal size distributions for an accurate assessment of mobility and reactivity, especially under slow flow conditions typical of field-scale problems.

Key words: particle size distribution, silver nanoparticles, mobility, dissolution, estimation error

Abbreviations used: RPA: representative (average) particle approach; NP: nanoparticles; nAg: silver NPs; CFT: clean-bed filtration theory; PSD: particle size distribution; SSA: specific surface area.

1. Introduction

Many varieties of anthropogenic nanoparticles (NPs) used in a wide array of industrial applications exhibit an intrinsic distribution of sizes. These include metallic nanoparticles (e.g., elemental silver [1], zero-valent iron [2], and TiO2 [3]) and non-metallic types such as fullerene [4] and graphene oxide [5] NPs. Also, a number of previous studies have demonstrated that the size distribution of NP suspensions can alter during transport [3,5] due to either agglomeration of suspended particles [3,6], ripening [7] (i.e. attachment to retained particles), or preferential filtration of particles of specific size due to the size-dependence of collector contact efficiency [8].

Size and surface state (i.e. surface area and surface functionalization) are among the most important properties that shape numerous anomalies in the environmental behavior of engineered NPs compared to traditional contaminants [9,10]. Potential toxicity of nanoparticles [11,12] as well as mechanisms that dictate their fate in terrestrial ecosystems (i.e. dissolution [13], reactivity [14], attachment to [8] / detachment from [15] collector grains, aggregation [16,17], and hetero-aggregation [18]) are affected, among other factors, by size of particles and particle size distribution [2].

Physicochemical filtration is considered as the likely removal mechanism for particles in the sub-micron to nanometer range [19] in saturated porous media. In this size range and under typical conditions of shallow aquifer environments, particle-collector surface (PC) interactions are governed by electrostatic repulsion and van der Waals forces (i.e. DLVO interactions [20,21]) and unfavorable attachment conditions prevail; that is, only a fraction of PC collisions results in deposition. Under certain conditions, an interplay between hydration [22], steric [23,24] and/or magnetic forces can also control PC interactions [25,26]. All of these surface interaction forces exhibit a first or higher order functional dependence on d_p (particle size) [27]. Classical "clean-bed" filtration theory (CFT) decouples the filtration process into two steps: (i) transport to collision sites at the collector surface, and (ii) deposition into an energy minimum for a fraction of collisions carrying enough kinetic energy to surpass the repulsive energy barrier between interacting surfaces, if present [28,29].

Under unfavorable conditions for deposition, the depth of the secondary energy well is directly proportional to particle size [8] resulting in fast reversible attachment mode by deposition in secondary minima, and retention due to surface charge heterogeneity [30]. A deviation from CFT predictions has been reported by numerous investigators for unfavorable attachment [8,31,32], where non-exponential particle deposition profiles have been documented [33]. Systematic experimental studies conducted with different-sized colloids suggest the controlling influence of secondary minimum deposition and surface charge heterogeneities on the observed deviation from colloid filtration theory [34]. In addition to the depth of the secondary energy well [8], the height of the electrostatic energy barrier [27] is also directly related to particle size. Here, not only is the transport to the collector surface affected by the size of a particle, but also the outcome of collisions can be determined by it; that is, irreversible 'slow' attachment of particles depositing in deep primary minima versus reversible 'fast' deposition in secondary minima.

Wang et al. [35] reported size effects on the retention of silica NPs which they attributed to two primary mechanisms: (a) direct effect on the interaction energies between NPs and sand surfaces, and (b) indirect effect on physicochemical properties such as zeta-potential thereby further affecting interaction energies and deposition behavior. Some studies report an increase in NP retention with size (e.g., Hahn et al. [36]) whereas others have demonstrated NP attachment efficiency independent of particle size [19]. Phenrat et al. [2] examined the effect of intrinsic particle size distribution (PSD) on the transport of surface-modified iron NPs and reported negligible effect of particle size on deposition in clean bed filtration under unfavorable deposition conditions. In contrast, Pelley and Tufenkji [37] examined the effect of particle size on NP mobility in laboratory-scale filtration experiments of latex NPs ranging in size between 50 to 1500 nm, and reported a mild increase of attachment efficiency (less than one order of magnitude) with size over a wide range of ionic strengths between 10 to 100 mM KCl. Similar trends (increased removal efficiency with particle size) have been reported for magnetic iron oxide NPs [38].

Despite an observed size dependence, the conventional approach for modeling filtration dynamics of particles with a size-distribution has been based on ensemble averaging where a distribution of sizes is

substituted by the diameter of a representative particle (referred herein to as the representative particle approach, RPA). Application of the RPA was the common practice (since the early work of Yao et al. [28] and Elimelech and O'Melia [29]) until more recent modeling attempts by Phenrat et al. [39] and Wang et al. [35]. The downside to consideration of the full range of PSD data in filtration modeling is the increased complexity and higher computational requirements of either (i) using a Lagrangian approach or (ii) discretizing the PSD through a probability mass function approach (pmf; a finite number of size classes (bins) and respective probabilities), solving the transport equation for each bin separately, and computing the weighted average of particle concentration using the pmf probability values [17]. The justification for adopting a more sophisticated modeling scheme will ultimately depend on the magnitude of the error introduced by the RPA. To the best of our knowledge the previous transport modeling studies that incorporate particle poly-dispersity [40,41,42] have not explored the error introduced by a Representative Particle Approximation.

In this work, our goal is to characterize the errors introduced in particle mobility and reactivity estimates for variably sized NP populations when the RPA is invoked. It is postulated that these errors could be significant based upon: the highly non-linear relationship between particle size and contact efficiency, particularly for complex particles undergoing complex heterogeneous chemical reactions. The study focuses on the coupled transport and dissolution of polydisperse silver NPs (nAg). Errors are quantified through examination of simulated spatiotemporal mass moments for (i) particulate and (ii) dissolved silver components. Experimental nAg mobility and dissolution data (Taghavy et al. [14]) and nAg PSD data from (Zhang et al. [1]) form the basis for these analyses. The transformation of nAg PSD during transport in porous media is also examined and the respective effects of flow velocity and filtration depth are evaluated.

2. Motivation and Theoretical Background for Error in RPA-Approximation

The particle size dependence of nAg deposition is rooted in the strong non-linear relationship between the single-collector contact efficiency, η_0 $(-)$ and particle hydrodynamic diameter, d_p (m), as illustrated in Figure 1. CFT theory predicts an optimum particle size at which a particle has the highest mobility. Above this optimal size, sedimentation and interception mechanisms and, below it, diffusive transport mechanisms increase the particle removal efficiency. Based upon this non-monotonic non-linear relationship, use of the RPA could lead to an under- or over-estimation of nAg retention for a polydisperse population, depending on the range of sizes within that population.

The nonlinear relationship between particle deposition rate and fractional surface coverage is another salient feature of colloid filtration dynamics that could lead to particle size distribution effects on particle deposition. This effect is based on a theoretical surface area exclusion phenomenon that creates a shadow zone on the collector surface down gradient of deposited particles [43,44] and has been confirmed by stagnation point flow cell studies [45]. However, predictions of particle size effects on the site-blocking process based on the so-called "shadow-zone" theory remain speculative in lieu of extensive experimental evidence to support a quantitative description of such effects. In the absence of appropriate supporting data, the effects of particle size distribution on site blocking and maximum attainable retention capacity [14] are neglected herein.

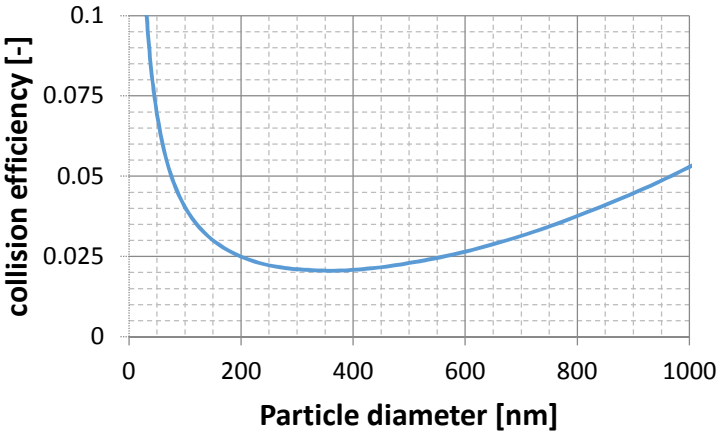

Figure 1. Single-collector contact efficiency calculated for nAg particles based on Tufenkji and Elimelech correlation [8] under experimental conditions of Taghavy et al. [14].

Dissolution is another important aspect of nAg fate that can be affected by particle size. The oxidative dissolution of nAg is a heterogeneous chemical reaction where reaction kinetic rate constant, k_{diss} (1/s), is a particle-specific parameter that depends on, among other factors, the available specific surface area, SSA (m^2/m^3), for the dissolution reaction:

$$k_{diss}(d_p) = \frac{k_{diss_0}}{SSA_0} \cdot SSA(d_p) \qquad \textit{Equation 1}$$

Here k_{diss_0} and SSA_0 are the pseudo-first order dissolution rate constant and specific surface area determined for a reference initial state, respectively. SSA is typically expressed as a linear function of inverse particle diameter for particles with regular geometric shape. For spherical particles, the SSA calculated based upon a representative particle size (SSA_{RPA}) can be compared to that calculated based upon the complete distribution of particle sizes (SSA_{PSD}). As shown in Appendix A of the supporting information (SI), the RPA-based estimator of SSA is negatively biased (See Appendix A of SI document for additional details):

$$SSA_{RPA} = \frac{6}{\rho_p \boldsymbol{d_p^m}} = \frac{6}{\rho_p \sum_i f_i^m \cdot d_{p_i}} \leq SSA_{PSD} = \frac{6}{\rho_p} \cdot \sum_i \frac{f_i^m}{d_{p_i}} \qquad \textit{Equation 2}$$

Where ρ_p (kg/m^3) is particle density, $\boldsymbol{d_p^m}$ (m) is mean particle diameter, and f_i^m is the mass fraction of particles in the size bin i, with d_{p_i} (m) denoting the bin-averaged diameter. This inequality indicates that use of a RPA will yield a systematic underestimation of particle reactivity (here dissolution kinetics) for surface reactions where specific surface area is a limiting factor.

3. Mathematical Modeling

Mathematical Model Implementation

A CFT adaptation of the random-walks particle-tracking modeling framework presented in Taghavy et al. [14] was implemented in this study. This modeling approach facilitates the evaluation of the influence of particle size distributions and their evolution in space/time. Mass balance for nAg, Ag^+ and dissolved oxygen was expressed using a set of advection-dispersion-reaction (ADR) equations with size-dependent constitutive relationships describing nAg deposition and dissolution (See Appendix B of SI document for detail). The hybrid Eulerian-Lagrangian simulator (HELP-1D) presented in Taghavy et al. [14] was modified to incorporate non-parametric size distributions for the influent particles at the inlet boundary, accepting any tabulated form as either a number-based or volumetric-based cumulative distribution function (cdf). Prior to introduction to the simulation domain, a random diameter was selected for each simulated particle where the probability for selection of d_{p_i} was equal to f_i^m. For RPA simulations an identical average diameter was assigned to all particles. Note that, after the release of particles at the inlet boundary, particle dissolution and deposition are two dynamic processes that can alter the nAg PSD. The effect of aggregation, another potential mechanism for a dynamic PSD, on particle sizes was neglected, consistent with the observed high stability of the nAg suspension relative to the time-scale of transport experiments of Taghavy et al. [14].

Defining the RPA Error

RPA error for parameter Θ (e.g., recovered silver mass in particulate or ionic form) is defined as:

$$\epsilon_{\Theta} = \frac{\Theta_{RPA}}{\Theta_{PSD}} - 1 \qquad \textit{Equation 3}$$

where Θ_{RPA} and Θ_{PSD} are Θ estimates based on the treatment of NPs as a monodisperse (MD) or polydisperse (PD) population, respectively. A positive ϵ_{Θ} indicates an overestimation by the RPA, and vice versa.

Selection of Model Parameters

The base case for simulations in this study follows the experimental steps outlined in Taghavy et al. [14] for transport tests on dissolving citrate-stabilized nAg at fixed pH 4 through 12cm 40-50 mesh Ottawa sand columns saturated with a 10mM $NaNO_3$ solution. In these experiments, a 3 pore volume (PV; a dimensionless measure of time equal to the hydraulic residence time of a porous system) pulse of 3 mg/L nAg suspension was injected at a pore velocity of ca. 6.8 m/day into the column and was followed by a 2 PV post-flush with particle-free 10mM $NaNO_3$ solution. The nAg mobility and dissolution parameters were selected consistent with fitted parameters reported therein. A complete list of model input parameters is provided in Table 1.

Figure 2 depicts the three particle size distributions used in the simulations. PSD#1 (mean particle diameter of ca. 39 nm) was adopted from Zhang et al. [1] for a citrate-stabilized nAg suspension measured at low ionic strength and near neutral pH. PSD#2 and PSD#3 are two illustrative distributions with identical mean particle size but different skewness and modality. PSD#2 was generated by rescaling the experimental PSD for 80 nm nAg from the same report [1] and adjusting the distribution mean to 39 nm (preserving the underlying variance) yielding a higher positive skewness than PSD#1. PSD#3 is a bimodal distribution that was generated consistent with the reported modality of PSDs for other metallic NPs (e.g., copper [46] and ZnO [47] NPs). Commonality of the mean size among the implemented PSDs means that the RPA prediction of the mobility and reactivity of NPs will be identical for particles following either of these distributions, that is, any variation in the difference between RPA simulations

and simulations that use full PSD data can be attributed solely to changes in the structural characteristics of the PSDs facilitating cross-simulation comparisons.

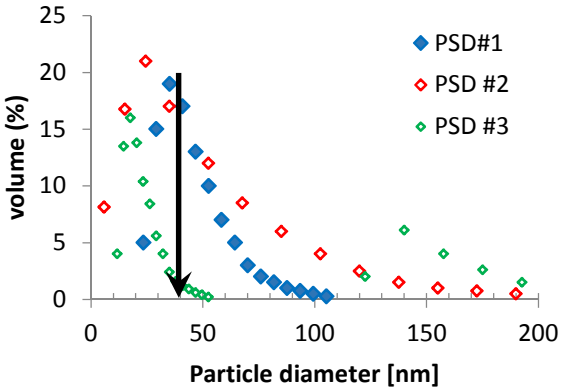

Figure 2. The experimental nAg PSD reported for nAg by Zhang et al. [1] *(in solid blue diamonds) and two generic unimodal and bimodal size distributions (open diamonds), all with an identical mean size of 39 nm.*

*Table 1. List of model input parameters for the base case simulation scenario, mostly selected consistent with Taghavy et al. (2013) report. For values taken from other reports, citations are provided under the reference column. * PV, the number of pore volumes, is a dimensionless measure of time.*

Property	symbol	unit	value	reference
attachment efficiency	α_{PC}	$-$	0.01	
mean influent particle diameter	d_p	nm	38.5	[1]
nAg dissolution coefficient	k_{nAg}^{diss}	$1/h$	3.45×10^{-2}	
normalized dissolution constant	k_{nAg}^{diss}/SSA_0	$g/m^2 \cdot h$	2.32×10^{-3}	
particle density	ρ_p	g/cm^3	10.49	
soil grain density	ρ_s	g/cm^3	2.65	
soil porosity	ϕ	$-$	0.37	
mean grain diameter	d_c	μm	354	
Hamaker constant, silver	A_{121}	$10^{-20}J$	1.02	[48]
Hamaker constant, silica	A_{323}	$10^{-20}J$	28.2	[49]
influent nAg concentration	$C_{0,nAg}$	mg/L	3.17	
influent Ag^+ concentration	C_{0,Ag^+}	mg/L	0.06	
influent DO concentration	C_{0,O_2}	mg/L	9.1	
column inner diameter	$I.D.$	cm	2.70	
column length	L_c	cm	12.1	
injected flow rate	Q_w	mL/min	1.0	
nAg pulse width		PV^*	2.88	

4. Results and Discussion

Size Distribution Effects on nAg Mobility

Figure 3.a-c presents the breakthrough curves for nAg and Ag+, and the total Ag retention profiles predicted for the monodisperse nAg with effective diameter of 39 nm and PSDs depicted in

Figure 2. According to simulation results for the base case, RPA error in terms of nAg recovery was minimal for the experimental PSD#1 (+3.2%) whereas nAg recovery prediction errors for PSD#2 and PSD#3 were +19.7% and +30.7% nAg, respectively (Figure 3.a). In contrast, Ag+ recovery prediction errors for the RPA were -13.5%, -58.1%, and -57.4% for PSDs #1, 2, and 3, respectively (Figure 3.b). Similarly, RPA prediction errors for total silver recovery for the base case were +2.4%, +11.3%, and +20.6% for the three PSDs. Thus, for this base case scenario, the RPA overestimates nAg and total Ag transport and consistently underestimates the transport of Ag^{+}, the more toxic form of silver [13,50]. In this scenario, the fate of total Ag was dominated by particulate Ag, consistent with a calculated Dahmkohler number (*Da*) of 0.018, Here *Da* is defined as the ratio of the time rate of nAg dissolution over the difference between the time rates of nAg advection and deposition:

$$Da_I = \frac{k_{diss}}{1/\tau_w - k_{att}} = \frac{k_{diss}}{v_w/L_c - \frac{3}{2}(1-\phi)v_w\alpha_{PC}\boldsymbol{\eta_0}/d_c} \qquad \textit{Equation 4}$$

Here τ_w (s), v_w (m/s), L_c (m), ϕ $(-)$, d_c (m), α_{PC} $(-)$, and $\boldsymbol{\eta_0}$ $(-)$ denote the residence time of water in the column, pore velocity, column length, porosity, median grain diameter, attachment efficiency, and single collector contact efficiency, respectively. Mean particle diameter was used to determine k_{diss} and k_{att} from Equation 1 and Equation A5 (SI-Appendix A).

Figures 3.d-f compares influent PSD curves with predicted effluent PSDs. Inspection of these plots reveals a slight preferential deposition of smaller particles for PSD#1, accompanied by an increase in the mean particle size from 39 nm to 40 nm between the inlet and outlet. This trend was more pronounced for the more highly skewed unimodal PSD#2 (49 nm at the outlet) and bimodal PSD#3 (54 nm at the outlet),where the effluent PSD clearly exhibits a reduction in volumetric percentages of particles in the lower quartiles, balanced by an increase in volumetric fractions in the upper quartiles. These model predictions are attributed to the dominance of Brownian diffusion as the main mechanism for removal of particles at the nanoscale; smaller particles exhibit higher diffusivity, and thus, higher removal efficiency.

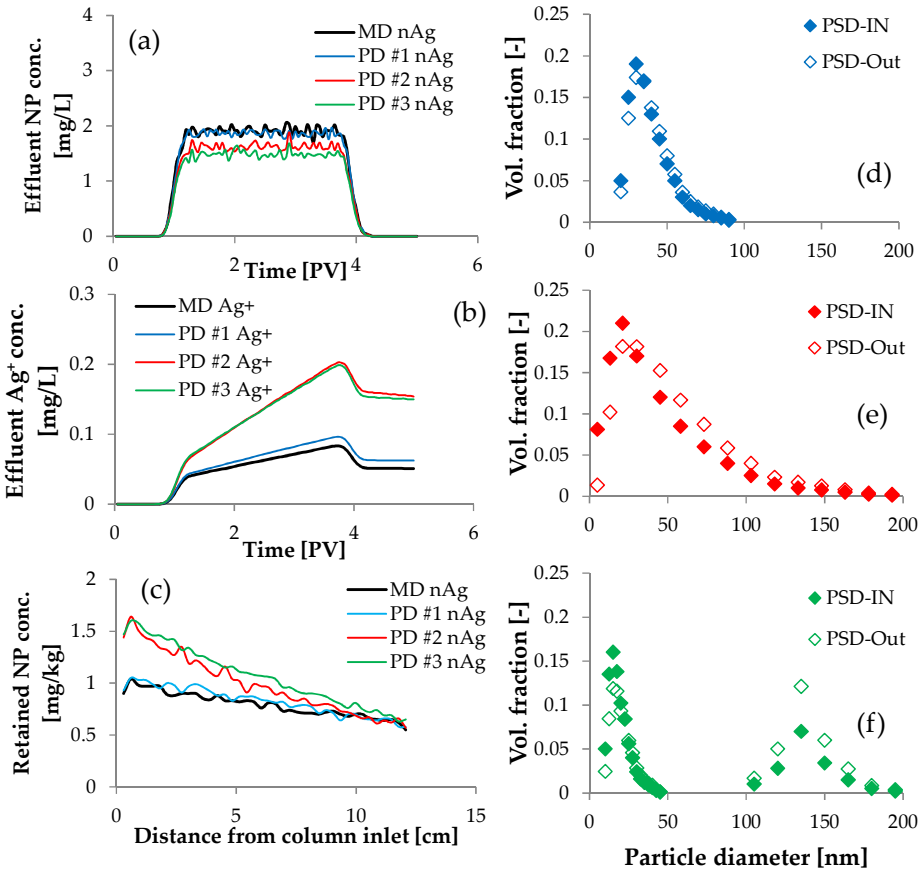

Figure 3. Simulated (a) nAg and (b) Ag^+ breakthrough curves and (c) nAg retention profiles based on RPA (MD: monodisperse – thick solid black lines) and polydisperse (PD) treatment of PSD#1-3 distributions all with identical mean particle diameter, and PSD diagrams of influent versus simulated effluent NPs for (d) experimental PSD #1, and generic (e) skewed unimodal PSD#2, and (f) bimodal PSD#3 distributions.

Influence of travel distance and flow velocity on RPA-approximation

The base case results presented above were characterized by a small filtration depth (12 cm) and high interstitial velocity (6.8 m/d) [14]). To explore the effects of filtration depth and flow velocity on prediction errors, two additional scenarios were considered: (i) a 2-fold increase of filtration length and (ii) a 10-fold reduction of pore velocity to 0.68 m/d, the mid-range of typical of groundwater velocity in shallow sandy aquifers [51]. In both cases a total of 234 µg nAg was injected, the same as used for the base-case.

Increased filter length. RPA simulations (based on a mean particle diameter of 39 nm) suggest that doubling the filtration length reduces nAg elution (from 61.5% (base) to 37.0%) and increases Ag^+ elution (from 2.6% to 4.1%) for all considered PSDs (also compare Figure 4.a and Figure 4.b). Similar trends

were also observed for predictions using the full PSDs. The RPA recovery prediction error associated with PSD#1 was +4.5%, -10.5% and +2.7% for nAg, Ag^+, and total Ag respectively. Comparisons with the respective error values for the base case (+3.2%, -13.5%, and +2.4% for nAg, Ag^+, and total Ag) reveals that a longer filtration length was associated with a slightly increasing (worsening) discrepancy in nAg mobility predictions and a decreasing (improving) estimate of Ag^+ speciation. Similar trends were found for the PSD #2 and bimodal PSD#3 distributions. In both cases, the RPA predicted error worsened for nAg (PSD#2: from +19.7% to +23.8%; PSD#3: from +30.7% to +47.9%) and improved for Ag^+ (PSD#2: from -58.1% to -47.6%; PSD#3: from -57.4% to -49.4%) when the filtration length was doubled (a comprehensive set of mass elution and RPA error data are presented in Appendix C – Tables A2 and A3 of SI document).

Reduced flow velocity. Decreasing pore velocity by one order-of-magnitude from the base case substantially reduced nAg mobility and enhanced silver ion speciation (compare Figure 4.a and Figure 4.c). The RPA predicts an order of magnitude decrease in nAg elution (from 61.5% to 6.3%) and a 13-fold increase in Ag^+ elution (from 2.6% to 34.3%). This decreased nAg mobility is attributed to two factors: (i) The dependence of contact efficiency on velocity (a ca. 5 fold increase for 39 nm sized particles (see Figure 5)) and (ii) An increase in nAg dissolution due to the increased contact time, consistent with the calculated Dahmkohler number of ~1.0 for this case (about 50 times greater than the respective value for the base case).

Another remarkable result is the prediction of a hyper-exponential spatial distribution of retained nAg for the PSDs #2 and 3 (Figure 6.c). It is important to emphasize that this predicted "non-exponential retention profile" is the result of incorporation of PSD data into a classical filtration model. The presence of a hyper-exponential retention profile has been interpreted in experimental studies as a deviance from CFT [52,53,54] and typically attributed to non-CFT mechanisms, such as physical straining [31] or non-Fickian transport behavior [53]. The present work demonstrates, however, how such profiles could arise for a variably sized NP population without invoking additional retention mechanisms.

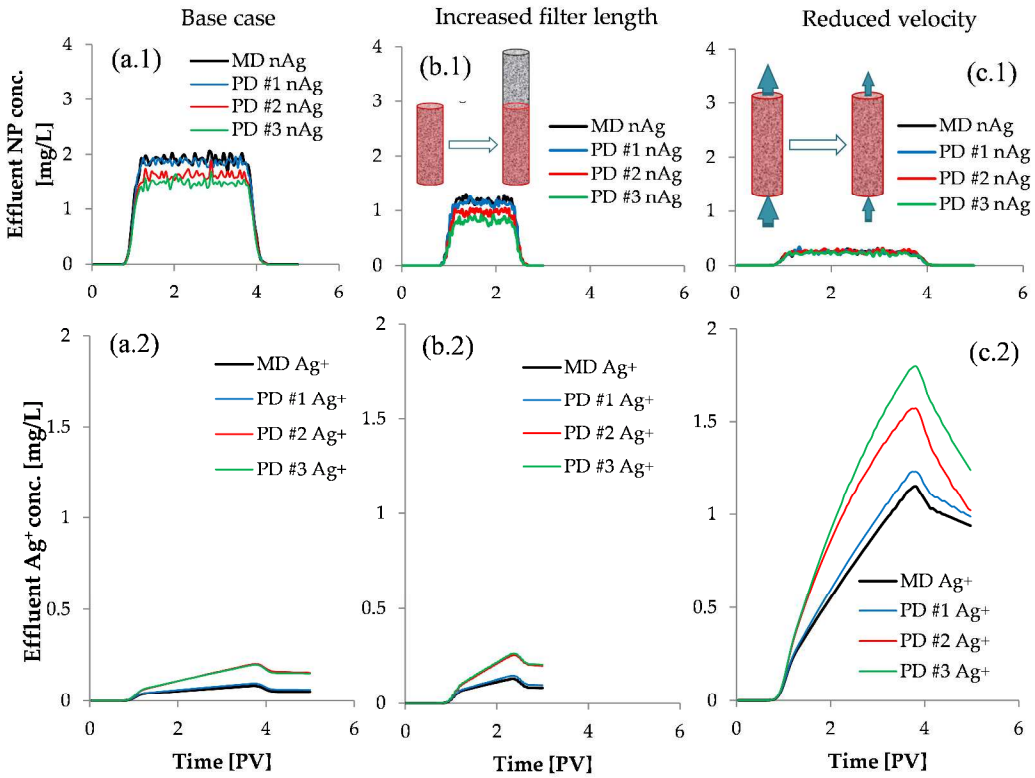

Figure 4. Simulated breakthrough curves of (1) nAg and (2) Ag^+ ions for the (a) base case, (b) 2-fold increase of filtration length, and (c) one order-of-magnitude reduction of flow velocity. A total silver mass of 234µg is injected in all simulated scenarios.

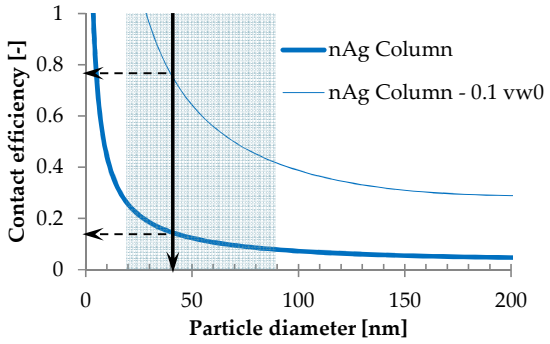

Figure 5. Single collector contact efficiency curves based on Tufenkji and Elimelech correlation for the base case (pore velocity of 6.8 m/d – thick line) and reduced velocity scenario (pore velocity of 0.68 m/d – thin line).

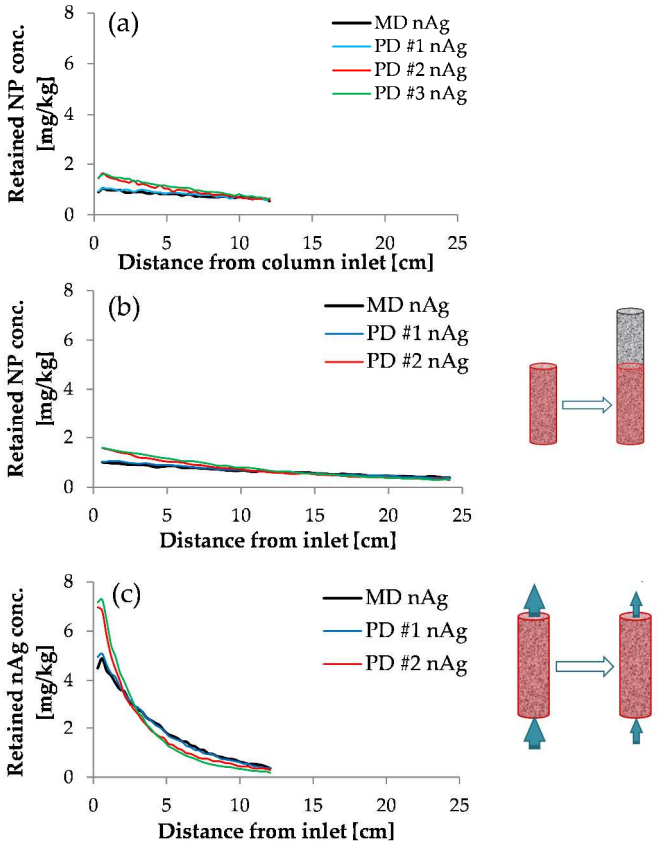

Figure 6. Simulated nAg retention profiles corresponding to the end of post flush period for (a) base case, (b) increased filter length, and (c) reduced velocity scenarios. A hyper-exponential structure is predicted in the latter scenario for the unimodal PSD#2 (high skew), and bimodal PSD#3 distributions.

A general negative bias in RPA predictions of both nAg mobility and Ag^{+} speciation was found for the implemented PSDs #1-3 at this lower velocity. Here RPA-error on total Ag recovery was -6.3% for the experimental PSD#1 and further increased in magnitude to -25.5% and -32.1% for generic PSD#2 and PSD#3, respectively (see SI Appendix C – Table A3 for further details). It is important to note the underestimation of silver transport in both particulate and dissolved forms for all simulated PSDs at low interstitial velocity, which implies a systematic underestimation of exposure to both toxins in risk assessment studies if analyses are based on the RPA approach. Nevertheless, the overall mobility estimation error was limited to ca. 6% based on the experimental particle size distribution (i.e. PSD#1).

Comparisons of influent PSDs with simulated effluent PSDs (Figure 7) reveals that the preferential filtration of smaller particles is intensified with either an increase in the filter length or decrease of flow velocity. This results in a growth of the mean particle size along the transport path

through the filter/porous media (mean effluent particle diameters of 42 nm and 47 nm for these two cases are predicted for experimental PSD#1). This effect is more pronounced for the PSD with higher skew (i.e. PSD#2 – Figure 7.b) and even more particularly, for the bimodal distribution (i.e. PSD#3 – Figure 7.c). A mean particle diameter of 121 nm was predicted for the reduced flow scenario for PSD#3, a staggering increase of more than 200% in the mean size with respect to the injected particles, i.e. 39 nm (see Appendix C – Table A4 of SI document for details). The important implications of this growth effect are (i) an increase in effective mobility of nAg after removal of smaller particles and (ii) a gradual decrease in nAg dissolution due to the lower SSA of the larger particles remaining in suspension. Thus, the subsurface mobility and longevity of polydisperse nAg are expected to increase with distance from the point of introduction.

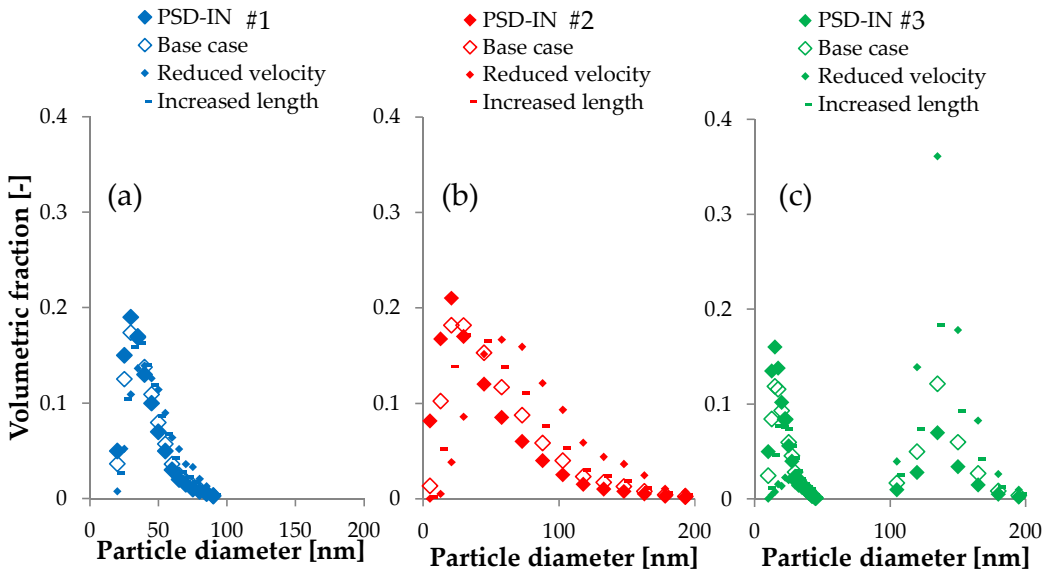

Figure 7. Influent (♦) and simulated effluent PSDs for (a) experimental PSD #1, and generic (b) skewed unimodal PSD#2 and (c) bimodal PSD#3 distributions, for the base case (◊), and increase filter length (-) and reduced velocity (small ♦) scenarios.

Effect of Structural Characteristics of Particle Size Distribution on RPA Error

In order to systematically characterize the effect of the shape characteristics of the PSD of polydisperse populations on the error associated with RPA estimates, the discrete experimental PSD#1was fitted to continuous lognormal distribution (fitted μ_{LN} and σ_{LN} of 3.58 and 0.36 – see Appendix D of SI document for detail) and the sensitivity of RPA-error to variations in distribution (i)

skewness and (ii) mean size was analyzed in terms of nAg mobility, Ag^+ speciation, and total Ag transport.

Sensitivity to Variations in Skewness. The skewness of the PSD#1 fitted lognormal distribution was parametrically estimated as 1.16, as a function of σ_{LN} (Equation 2.c – Appendix D of SI document). The sensitivity of predicted particulate and dissolved silver elution was analyzed within a two order-of-magnitude range of variation from 0.1- to 10-fold of PSD#1 skewness (Figure A3 – Appendix D of SI document). Distribution mean was kept at a constant 39 nm in this set of simulations. A positive correlation was predicted between the distribution skewness and the magnitude of RPA error in both nAg and Ag^+ elution estimates (Figure 8.a). It was also found that, as skewness increased, the RPA overestimated nAg mobility (conservative) which was contrary to the consistent underestimation of more toxic dissolved silver elution. Lowering the skewness by one order of magnitude, on the other hand, resulted in a diminishing of RPA error in both nAg and Ag^+ elution estimates to +0.01% and -0.4%, respectively.

Sensitivity to Variations in Mean Size. A two order-of-magnitude range of variation of distribution mean between 4 nm to 390 nm was simulated and model sensitivity in terms of nAg and Ag+ elution was evaluated based on RPA and PSD approaches (Figure A3.b – Appendix D of SI document). The distribution skewness was held constant at a parametric value of 1.16 consistent with the log-normal fit to PSD#1. The estimate of RPA error in nAg mobility asymptotically decreased from +3.2% to +2% with the increase of mean particle size from 39 nm to 390 m. In contrast, with a decrease of mean diameter from 39, the error first increased to a maximum +4.8% (20 nm) but then decreased to -7.7% (4 nm). Varying the mean diameter affected the RPA-error for the prediction of Ag^+ elution to a lesser extent; a one order-of-magnitude increase and decrease of mean diameter both reduced error magnitude (from -13.5% to about -11%) (Figure 8.b). In absolute terms, a comparison of FiguresFigure 8.a and Figure 8.b reveals that both types of RPA error showed lower sensitivity to variations in distribution mean compared to skewness.

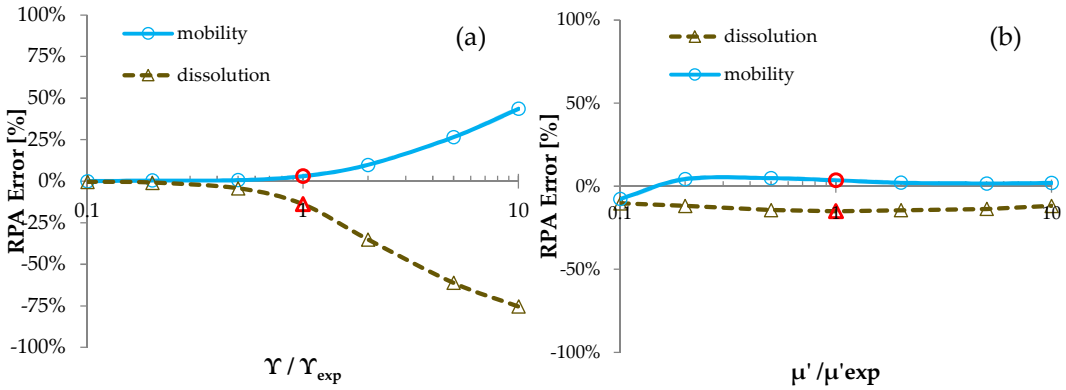

Figure 8. Sensitivity of predicted RPA error in the estimates of nAg mobility (blue solid lines) and Ag^+ transport (brown dashed lines) to variations in (a) distribution skewness at constant mean particle diameter (39 nm) and (b) distribution mean at constant coefficient of variation of 0.37.

5. Conclusion

In this study, a systematic bias was found in RPA estimates of nAg dissolution, where Ag^+ speciation and elution were methodically underestimated. Developments for mitigation of the RPA error in nAg mobility estimation appears particularly challenging, as RPA both under- and overestimated nAg elution depending on the specific properties of particles, flow, and porous medium. The RPA-approximation remained within a ~10% margin of error in all case scenarios associated with the actual experimental particle size distribution PSD#1 (blue bars in Figure 9). The magnitude of RPA-error positively correlated with filter length without affecting the overall trend predicted for the base case in terms of overestimation of nAg and total Ag elution (Figure 9.a andFigure 9.Figure 9b). Reducing flow velocity resulted in a transitioning in the controlling role of particulate silver to that of dissolved silver in determining the fate of total Ag. A reduction in flow velocity also altered the RPA-prediction error pattern, resulting in underestimation of silver elution in both forms for all simulated PSDs (Figure 9.c). It was also predicted that a (i) generic increase in the skewness or (ii) bimodal structure of the PSD can intensify RPA-related errors. The former conclusion was confirmed by a subsequent sensitivity analysis where a positive correlation was found between distribution skewness and the magnitude of RPA error in the estimates of both nAg and Ag^+ elution.

The model predictions of nAg dissolution presented herein are based on an assumption regarding the acidity of the subsurface environment (i.e. pH 4 used in Taghavy et al. [14] experiments), a condition representative only of acidic soils [55] or some landfill sites [56]. Thus, the findings cannot be generalized to natural well-buffered soil systems. It should also be noted that polydispersity of particle sizes can also affect the surface capacity of soil grain collectors for NP retention thereby further influencing NP mobility estimates and the respective RPA-error. This effect, however, cannot be predicted with the classical clean-bed filtration theory, and is, thus, beyond the scope of this study. Characterizing the error in RPA estimates of NP mobility for NP suspension – porous medium systems that exhibit a limited retention capacity for particle attachment could be carried out as a continuation of this work through the implementation of predictions of "shadow-zone" theory [43] on the scaling of maximum retention capacity with particle size. A comprehensive assessment of the accuracy of RPA versus PSD-based methods will be contingent upon the characterization of the influence of size effects not only on the attachment efficiency (this work) but also on the extent of particle-collector attachment.

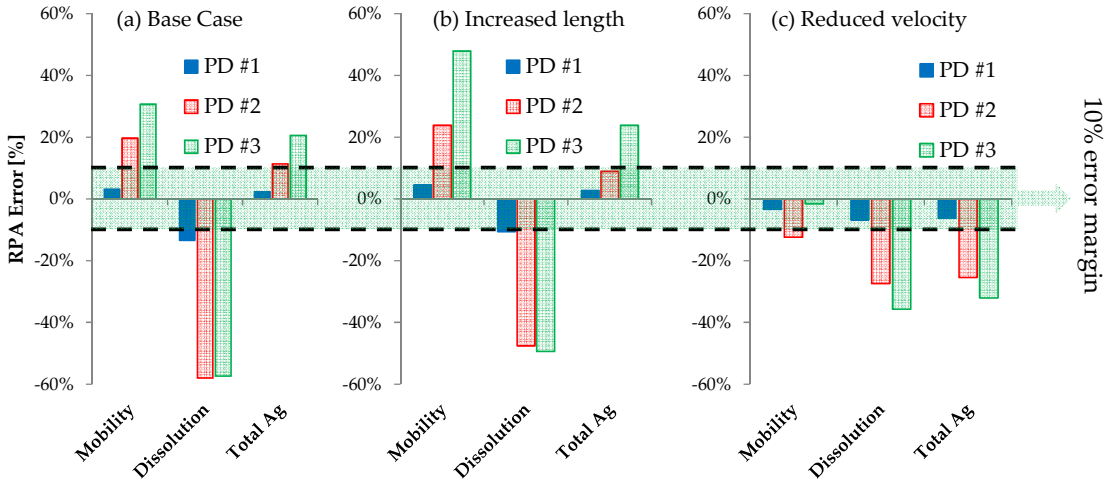

Figure 9. Bar plots of RPA error in estimation of nAg, Ag+, and total Ag elution, predicted for the (a) base case, (b) increased filter length, and (c) reduced flow scenarios.

Acknowledgments: This work was partly supported by the faculty startup fund provided by the College of Engineering of the University of Massachusetts Dartmouth. The authors wish to acknowledge the support provided by a grant from the National Science Foundation, Award no. CBET-0854136. The work has not been subject to NSF review, and therefore, does not necessarily reflect the views of the organization and no official endorsement should be inferred.

Conflict of Interest: The authors declare that they have no conflict of interest.

References

1. Zhang, W., Yao, Y., Sullivan, N. & Chen, Y., Modeling the primary size effects of citrate-coated silver nanoparticles on their ion release kinetics. *Environmental science & technology* **45** (10), 4422-4428 (2011).

2. Phenrat, T. *et al.*, Particle size distribution, concentration, and magnetic attraction affect transport of polymer-modified Fe0 nanoparticles in sand columns. *Environmental science & technology* **43** (13), 5079-5085 (2009).

3. Solovitch, N. *et al.*, Concurrent aggregation and deposition of TiO2 nanoparticles in a sandy porous media. *Environmental Science & Technology* **44** (13), 4897-4902 (2010).

4. Brant, J., Lecoanet, H. & Wiesner, M. R., Aggregation and deposition characteristics of fullerene nanoparticles in aqueous systems.. *Journal of Nanoparticle Research* **7** (4-5), 545-553 (2005).

5. Sun, Y., Gao, B., Bradford, S. A., Wu, L. & Wu, J., Transport, retention, and size perturbation of graphene oxide in saturated porous media: Effects of input concentration and grain size. *Water research* **68**, 24-33 (2015).

6. Jiang, X., Tong, M., Lu, R. & Kim, H., Transport and deposition of ZnO nanoparticles in saturated porous media. *Colloids and Surfaces A: Physicochemical and Engineering Aspects* **401**, 29-37 (2012).

7. Tong, M., Ma, H. & Johnson, W. P., Funneling of flow into grain-to-grain contacts drives colloid− colloid aggregation in the presence of an energy barrier.. *Environmental science & technology* **42** (8), 2826-2832 (2008).

8. Tufenkji, N. & Elimelech, M., Correlation equation for predicting single-collector efficiency in physicochemical filtration in saturated porous media. *Environmental Science & Technology* **38** (2), 529-536 (2004).

9. Garner, K. L. & Keller, A. A., Emerging patterns for engineered nanomaterials in the environment: a review of fate and toxicity studies. *Journal of Nanoparticle Research* **16** (8), 1-28 (2014).

10. Darlington, T. K., Neigh, A. M., Spencer, M. T., Guyen, O. T. & Oldenburg, S. J., Nanoparticle characteristics affecting environmental fate and transport through soil. *Environmental Toxicology and Chemistry* **28** (6), 1191-1199 (2008).

11. Tiede, K. *et al.*, Detection and characterization of engineered nanoparticles in food and the environment.. *Food Additives and Contaminants* **25** (7), 795-821 (2008).

12. Warheit, D. B. *et al.*, Development of a base set of toxicity tests using ultrafine TiO 2 particles as a component of nanoparticle risk management. *Toxicology letters* **171** (3), 99-110 (2007).

13. Liu, J. & Hurt, R. H., Ion release kinetics and particle persistence in aqueous nano-silver colloids. *Environmental science & technology* **44** (6), 2169-2175 (2010).

14. Taghavy, A., Mittelman, A., Wang, Y., Pennell, K. D. & Abriola, L. M., Mathematical modeling of the transport and dissolution of citrate-stabilized silver nanoparticles in porous media. *Environmental*

science & technology **47** (15), 8499-8507 (2013).

15. Sen, T. K. & Khilar, K. C., Review on subsurface colloids and colloid-associated contaminant transport in saturated porous media.. *Advances in colloid and interface science* **119** (2), 71-96 (2006).

16. Sun, Y. *et al.*, Transport, retention, and size perturbation of graphene oxide in saturated porous media: Effects of input concentration and grain size. *Water research* **68**, 24-33 (2015).

17. Raychoudhury, T., Tufenkji, N. & Ghoshal, S., Aggregation and deposition kinetics of carboxymethyl cellulose-modified zero-valent iron nanoparticles in porous media. *Water research* **46** (6), 1735-1744 (2012).

18. Praetorius, A., Scheringer, M. & Hungerbühler, K., Development of Environmental Fate Models for Engineered Nanoparticles: A Case Study of TiO2 Nanoparticles in the Rhine River. *Environmental science & technology* **46** (12), 6705-6713 (2012).

19. Elimelech, M., Predicting collision efficiencies of colloidal particles in porous media. *Water Research* **26** (1), 1-8 (1992).

20. Derjaguin, B. V. & Landau, L., Theory of the stability of strongly charged lyophobic sols and of the adhesion of strongly charged particles in solutions of electrolytes. *Acta physicochim. URSS,* **14** (6), 633-662 (1941).

21. Verwey, E. J. W. & Overbeek, J. T. G., *Stability of lyophobic colloids* (Elsevier, Amsterdam, 1948).

22. Labille, J. *et al.*, Hydration and dispersion of C60 in aqueous systems: The nature of water− fullerene interactions. *Langmuir* **25** (19), 11232-11235 (2009).

23. Byrd, T. L. & Walz, J. Y., Interaction force profiles between Cryptosporidium parvum oocysts and silica surfaces. *Environmental science & technology* **39** (24), 9574-9582 (2005).

24. Alexander, S., Adsorption of chain molecules with a polar head a scaling description. *Journal De Physique* **38** (8), 983-987 (1977).

25. Baldassarre, F., Cacciola, M. & Ciccarella, G., A predictive model of iron oxide nanoparticles flocculation tuning Z-potential in aqueous environment for biological application. *Journal of Nanoparticle Research* **17** (9), 1-21 (2015).

26. De Vicente, J., Delgado, A. V., Plaza, R. C., Durán, J. D. G. & González-Caballero, F., Stability of cobalt ferrite colloidal particles. Effect of pH and applied magnetic fields. *Langmuir* **16** (21), 7954-7961 (2000).

27. Petosa, A. R., Jaisi, D. P., Quevedo, I. R., Elimelech, M. & Tufenkji, N., Aggregation and deposition of engineered nanomaterials in aquatic environments: role of physicochemical interactions. *Environmental science & technology* **44** (17), 6532-6549 (2010).

28. Yao, K. M., Habibian, M. T. & O'Melia, C. R., Water and waste water filtration. Concepts and applications. *Environmental science & technology* **5** (11), 1105-1112 (1971).

29. Elimelech, M. & O'Melia, C. R., Kinetics of deposition of colloidal particles in porous media. *Environmental science & technology* **24** (10), 1528-1536 (1990).

30. Redman, J. A., Walker, S. L. & Elimelech, M., Bacterial adhesion and transport in porous media: Role of the secondary energy minimum. *Environmental Science & Technology* **38** (6), 1777-1785 (2004).

31. Bradford, S. A., Yates, S. R., Bettahar, M. & Simunek, J., Physical factors affecting the transport and fate of colloids in saturated porous media. *Water Resources Research*, 38 (12) (2002).

32. Redman, J. A., Grant, S. B., Olson, T. M. & Estes, M. K., Pathogen filtration, heterogeneity, and the potable reuse of wastewater.. *Environmental science & technology* **35** (9), 1798-1805 (2001).

33. Bradford, S. A., Bettahar, M., Simunek, J. & Van Genuchten, M. T., Straining and attachment of colloids in physically heterogeneous porous media. *Vadose Zone Journal* **3** (2), 384-394 (2004).

34. Tufenkji, N. & Elimelech, M., Breakdown of colloid filtration theory: Role of the secondary energy minimum and surface charge heterogeneities. *Langmuir* **21** (3), 841-852 (2005).

35. Wang, C. *et al.*, Retention and transport of silica nanoparticles in saturated porous media: effect of concentration and particle size. *Environmental science & technology* **46** (13), 7151-7158 (2012).

36. Hahn, M. W. & O'Melia, C. R., Deposition and reentrainment of Brownian particles in porous media under unfavorable chemical conditions: Some concepts and applications. *Environmental science & technology* **338** (1), 210-220 (2004).

37. Pelley, A. J. & Tufenkji, N., Effect of particle size and natural organic matter on the migration of nano-and microscale latex particles in saturated porous media.. *Journal of Colloid and Interface Science* **321** (1), 74-83 (2008).

38. Ying, T. Y., Yiacoumi, S. & Tsouris, C., High-gradient magnetically seeded filtration.. *Chemical Engineering Science* **55** (6), 1101-1113 (2000).

39. Phenrat, T., Kim, H. J., Fagerlund, F., Illangasekare, T. & Lowry, G. V., Empirical correlations to estimate agglomerate size and deposition during injection of a polyelectrolyte-modified Fe 0 nanoparticle at high particle concentration in saturated sand. *Journal of contaminant hydrology* **118** (3), 152-164 (2010).

40. Ma, E. *et al.*, Modeling of the transport and deposition of polydispersed particles: Effects of hydrodynamics and spatiotemporal evolution of the deposition rate. *Environmental Pollution* **237**, 1011-1022 (2018).

41. Bradford, S. A. & Toride, N., A stochastic model for colloid transport and deposition. *Journal of environmental quality* **36** (5), 1346-1356 (2007).

42. Meesters, J. A., Koelmans, A. A., Quik, J. T., Hendriks, A. J. & van de Meent, D., Multimedia modeling of engineered nanoparticles with SimpleBox4nano: model definition and evaluation. *Environmental science & technology* **48** (10), 5726-5736 (2014).

43. Ko, C. H. & Elimelech, M., The "shadow effect" in colloid transport and deposition dynamics in granular porous media: measurements and mechanisms. *Environmental science & technology* **34** (17), 3681-3689 (2000).

44. Li, Y., Wang, Y., Pennell, K. D. & Abriola, L. M., Investigation of the transport and deposition of fullerene (C60) nanoparticles in quartz sands under varying flow conditions. *Environ. Sci. Technol.* **42**, 7174-7180 (2008).

45. Böhmer, M. R., van der Zeeuw, E. A. & Koper, G. J., Kinetics of particle adsorption in stagnation point flow studied by optical reflectometry. *Journal of colloid and interface science* **197** (2), 242-250 (1998).

46. Jones, E. H. & Su, C., Fate and transport of elemental copper (Cu 0) nanoparticles through saturated porous media in the presence of organic materials. *Water Research* **46** (7), 2445-2456 (2012).

47. Segets, D., Gradl, J., Taylor, R. K., Vassilev, V. & Peukert, W., Analysis of optical absorbance spectra for the determination of ZnO nanoparticle size distribution, solubility, and surface energy. *ACS nano* **3** (7), 1703-1710 (2009).

48. Bergström, L., Hamaker constants of inorganic materials. *Advances in colloid and interface science* **70**, 125-169 (1997).

49. Israelechvili, J., *Intermolecular and Surface Forces, 2nd Edn* (Academic Press, London, 1992).

50. Kittler, S., Greulich, C., Diendorf, J., Köller, M. & Epple, M., Toxicity of silver nanoparticles increases during storage because of slow dissolution under release of silver ions. *Chemistry of Materials* **22** (16), 4548-4554 (2010).

51. Kunkel, R. & Wendland, F., WEKU–a GIS-supported stochastic model of groundwater residence times in upper aquifers for the supraregional groundwater management. *Environmental Geology* **30** (1), 1-9 (1997).

52. Tufenkji, N. & Elimelech, M., Deviation from the classical colloid filtration theory in the presence of repulsive DLVO interactions. *Langmuir* **20** (25), 10818-10828 (2004).

53. Yuan, H. & Shapiro, A. A., Modeling non-Fickian transport and hyperexponential deposition for deep bed filtration. *Chemical Engineering Journal* **162** (3), 974-988 (2010).

54. Jiang, X., Tong, M., Lu, R. & Kim, H., Transport and deposition of ZnO nanoparticles in saturated porous media. *Colloids and Surfaces A: Physicochemical and Engineering Aspects* **401**, 29-37 (2012).

55. McLean, E. O., in *Methods of soil analysis. Part 2. Chemical and microbiological properties* (199-224, 1982).

56. Wise, M. G., McArthur, J. V. & Shimkets, L. J., Methanotroph diversity in landfill soil: isolation of novel type I and type II methanotrophs whose presence was suggested by culture-independent 16S ribosomal DNA analysis. *Applied and Environmental Microbiology* **65** (11), 4887-4897 (1999).

366

367